Structural Comparison of MTA Phosphorylase and MTA/AdoHcy Nucleosidase Explains Substrate Preferences and Identifies Regions Exploitable for Inhibitor Design†

Jeffrey E. Lee,[‡,§,||] Ethan C. Settembre,[‡,⊥] Kenneth A. Cornell,[#,△] Michael K. Riscoe,[#,△,○] Janice R. Sufrin,[▽] Steven E. Ealick,[⊥] and P. Lynne Howell*[,§,||]

Structural Biology and Biochemistry, Research Institute, Hospital for Sick Children, 555 University Avenue, Toronto, Ontario M5G 1X8, Canada, Department of Biochemistry, Faculty of Medicine, University of Toronto, Medical Sciences Building, Toronto, Ontario M5S 1A8, Canada, Department of Chemistry and Chemical Biology, Cornell University, Ithaca, New York 14853, Department of Chemistry, Portland State University, P.O. Box 751, Portland, Oregon 97207, Department of Biochemistry and Molecular Biology and Division of Vascular Surgery, Oregon Health Sciences University, 3181 SW Sam Jackson Park Road, Portland, Oregon 97201, Medical Research Service, 151-0, Veterans Affairs Medical Center, 3710 SW US Veterans Hospital Road, Portland, Oregon 97021, and Department of Pharmacology and Therapeutics, Roswell Park Cancer Institute, Elm and Carlton Streets, Buffalo, New York 14263

Received August 20, 2003; Revised Manuscript Received January 9, 2004

ABSTRACT: The development of new and effective antiprotozoal drugs has been a difficult challenge because of the close similarity of the metabolic pathways between microbial and mammalian systems. 5′-Methylthioadenosine/*S*-adenosylhomocysteine (MTA/AdoHcy) nucleosidase is thought to be an ideal target for therapeutic drug design as the enzyme is present in many microbes but not in mammals. MTA/AdoHcy nucleosidase (MTAN) irreversibly depurinates MTA or AdoHcy to form adenine and the corresponding thioribose. The inhibition of MTAN leads to a buildup of toxic byproducts that affect various microbial pathways such as quorum sensing, biological methylation, polyamine biosynthesis, and methionine recycling. The design of nucleosidase-specific inhibitors is complicated by its structural similarity to the human MTA phosphorylase (MTAP). The crystal structures of human MTAP complexed with formycin A and 5′-methylthiotubercidin have been solved to 2.0 and 2.1 Å resolution, respectively. Comparisons of the MTAP and MTAN inhibitor complexes reveal size and electrostatic potential differences in the purine, ribose, and 5′-alkylthio binding sites, which account for the substrate specificity and reactions catalyzed. In addition, the differences between the two enzymes have allowed the identification of exploitable regions that can be targeted for the development of high-affinity nucleosidase-specific inhibitors. Sequence alignments of *Escherichia coli* MTAN, human MTAP, and plant MTA nucleosidases also reveal potential structural changes to the 5′-alkylthio binding site that account for the substrate preference of plant MTA nucleosidases.

Drug resistance among pathogens and the emergence of "superbugs" resistant to even the most potent antibiotic are of considerable concern in the medical community. This problem is compounded as few new classes of antibiotics have been introduced in the last 20 years. The urgent need to find new antimicrobial targets and novel antimicrobial therapeutics that are capable of eliminating the pathogen without harm to the host is of great importance. The design of such drugs requires the identification of metabolic differences between the pathogen and host. One such exploitable target is the enzyme 5′-methylthioadenosine/*S*-adenosylhomocysteine (MTA/AdoHcy)[1] nucleosidase (MTAN) (*1*, *2*). MTA/AdoHcy nucleosidase (EC 3.2.2.9) is a dual substrate-specific enzyme that irreversibly cleaves both MTA and AdoHcy to form adenine and the corresponding thioribose, 5′-methylthioribose (MTR) and *S*-ribosylhomocysteine (SRH), respectively (*3*).

MTA/AdoHcy nucleosidase is present in many pathogenic microbes such as *Staphylococcus aureus*, *Salmonella typhimurium*, *Enterococcus faecalis*, *Streptococcus pyogenes*,

† This work is supported by research grants from the Canadian Institute for Health Research (CIHR 43998), the U.S. Department of Agriculture (02-0047), the US Veterans Affairs Medical Research Program, the W. M. Keck Foundation, and the Lucille P. Markey Charitable Trust. J.E.L. and P.L.H. are the recipients of a CIHR graduate scholarship and CIHR investigator award, respectively.

* To whom correspondence should be addressed. Phone: (416) 813-5378. E-mail: howell@sickkids.ca.

‡ These authors contributed equally to the work described.

§ Hospital for Sick Children.

|| University of Toronto.

⊥ Cornell University.

Portland State University.

△ Oregon Health Sciences University.

○ Veterans Affairs Medical Center.

▽ Roswell Park Cancer Institute.

[1] Abbreviations: MTA, 5′-methylthioadenosine; AdoHcy, *S*-adenosylhomocysteine; MTAP, 5′-methylthioadenosine phosphorylase; MTAN, 5′-methylthioadenosine/*S*-adenosylhomocysteine nucleosidase; MTR, 5′-methylthioribose; AI-2, autoinducer 2; MTR 1-P, 5′-methylthioribose 1-phosphate; FMA, formycin A; MTT, 5′-methylthiotubercidin; SRH, *S*-ribosylhomocysteine.

10.1021/bi035492h CCC: $27.50
Published on Web 04/10/2004

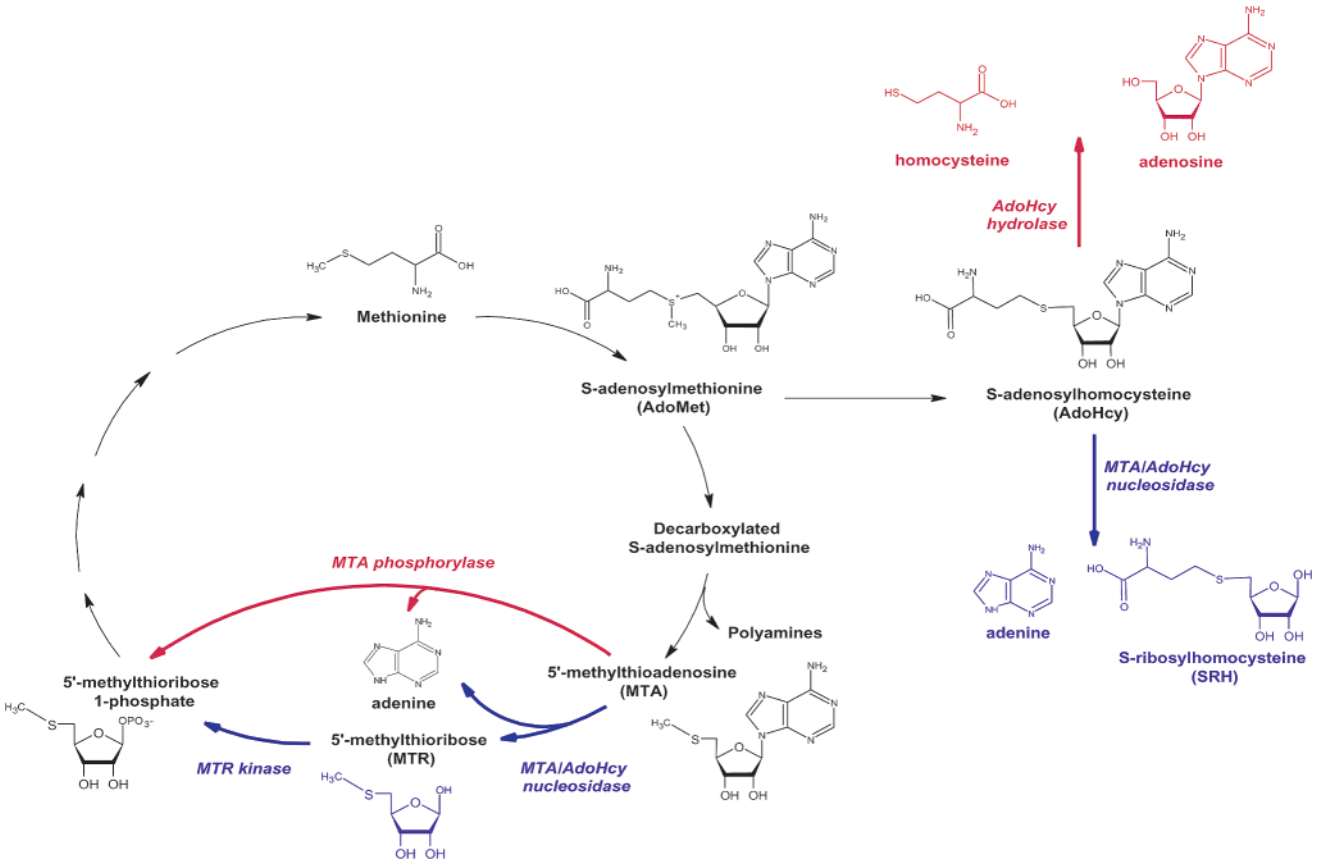

FIGURE 1: Mammalian and microbial catabolic pathways for 5′-methylthioadenosine (MTA) and *S*-adenosylhomocysteine (AdoHcy). Mutually exclusive mammalian and microbial metabolic pathways are highlighted in red and blue, respectively.

Streptococcus pneumoniae, *Mycobacterium tuberculosis*, *Haemophilus influenzae*, and *Bacillus anthracis* but not in mammalian cells. The nucleosides MTA and AdoHcy are catabolized in mammals and microbes by two mutually exclusive mechanisms (Figure 1). In mammalian systems, the breakdown of MTA and AdoHcy requires two separate enzymes. MTA is catabolized in a reversible reaction to adenine and 5′-methylthioribose 1-phosphate (MTR 1-P) by MTA phosphorylase, while AdoHcy is broken down by AdoHcy hydrolase to homocysteine and adenosine (*4*). In contrast, most microbes that lack MTA phosphorylase or AdoHcy hydrolase utilize the dual substrate specificity of MTA/AdoHcy nucleosidase to cleave the ribosidic linkage in AdoHcy and MTA.

The inhibition of MTAN allows the buildup of the two toxic nucleosides, MTA and AdoHcy (Figure 1). The buildup of MTA acts as a potent feedback inhibitor of spermidine synthase, which is involved in polyamine biosynthesis (*5*, *6*). Polyamines are thought to play a key role in growth processes and in the regulation of DNA synthesis. Furthermore, the impairment of MTAN blocks the methionine recycling pathway as MTA is not able to be recycled back to methionine (*1*, *2*). The salvaging of methionine is important because methionine is an essential amino acid that is energetically expensive to synthesize. The buildup of the second nucleoside, AdoHcy, results in a potent feedback inhibition of AdoMet-dependent transmethylation reactions (*7*). In addition, buildup of AdoHcy leads to disruption of the autoinducer 2 (AI-2) bacterial quorum sensing pathway, which has been implicated in the regulation of virulence factors (*8*−*10*) and the formation of biofilms (*11*) in many bacteria. *S*-Ribosylhomocysteine generated by MTAN is converted to AI-2 by the enzyme LuxS (*12*, *13*).

MTA/AdoHcy nucleosidase was verified as a good antibacterial target using MTAN null mutants generated in the pathogenic and nonpathogenic bacteria *Escherichia coli*, *S. typhimurium*, *H. influenza*, *E. faecalis*, *S. pyogenes*, and *S. pneumoniae* (*14*). Isolated *E. coli* and *S. typhimurium* null mutants exhibited an attenuated growth profile, an inability to synthesize the AI-2 autoinducer, and an altered carbohydrate utilization profile. In addition, the *S. typhimurium* MTAN null mutant resulted in a decrease in virulence and had proliferation deficiencies compared to the parental strain. Null MTAN mutants of *H. influenza*, *E. faecalis*, *S. pyogenes*, and *S. pneumoniae* could not be isolated, suggesting that in these bacteria MTAN is critical.

The structures of MTAP complexed to adenine and MTA-sulfate (*15*) and MTAN complexed to adenine, formycin A (FMA), and 5′-methylthiotubercidin (MTT) (*16*, *17*) have been reported previously. We present here the crystal structures of the human MTAP complexed to FMA and MTT. The MTAP−FMA- and MTAP−MTT-bound structures allow the first detailed active site comparison of MTAP with their MTAN inhibitor counterparts. The comparisons of MTAN and MTAP have identified structural differences in the purine, ribose, and 5′-alkylthio binding sites that explain the binding preferences of substrates and inhibitors in MTAP and MTAN. Such comparative studies are necessary in the drug design process, as exploitable structural and electrostatic differences need to be identified if inhibitors specific to the nucleosidase are to be designed. Furthermore, the importance of certain residues in the active sites

Table 1: Data Collection and Refinement Statistics

	MTAP complex	
	FMA	MTT
Diffraction Statistics		
space group	*P*321	*P*321
a (Å)	121.0	119.5
c (Å)	44.2	44.2
wavelength (Å)	1.000	1.000
no. of observed reflections	177155	104348
no. of unique reflections	25569	19929
resolution range (Å)	20.0−2.03	20.0−2.10
R_{merge} (%)[a]	4.8 (5.3)[b]	4.6 (10.6)[c]
redundancy	6.9	5.2
completeness (%)	99.9 (99.5)[b]	94.0 (75.0)[c]
$I/\sigma(I)$	36.8 (8.0)[b]	29.9 (6.7)[c]
Refinement Statistics		
no. of reflections	25305	19929
no. of reflections in test set	1728	1390
resolution range (Å)	20.0−2.03	20.0−2.10
R_{cryst} (%)[d]	18.0	18.6
R_{free} (%)[e]	19.8	20.7
overall *B*-factor (Å^2)		
main chain	16.4	27.9
side chain	19.6	30.7
ligand	16.4	23.1
sulfate	n/a	28.5
water	32.2	37.2
rms deviation		
bonds (Å)	0.005	0.005
angles (deg)	1.22	1.23

[a] $R_{merge} = \sum\sum|I(k) - \langle I\rangle|/\sum I(k)$, where $I(k)$ and $\langle I\rangle$ represent the diffraction intensity values of the individual measurements and the corresponding mean values. The summation is over all unique measurements. [b] Values given in parentheses refer to reflections in the outer resolution shell: 2.13−2.03 Å. [c] Values given in parentheses refer to reflections in the outer resolution shell: 2.15−2.10 Å. [d] $R_{cryst} = \sum_{hkl}||F_o| - k|F_c||/\sum|F_o|$, where F_o and F_c are the observed and calculated structure factors, respectively. [e] For R_{free} the sum is extended over a subset of reflections (7%) excluded from all stages of the refinement.

combined with a sequence alignment of *E. coli* MTAN and MTA nucleosidase from plants provides preliminary insight into the substrate preferences of the plant enzymes.

MATERIALS AND METHODS

Protein Preparation, Crystallization, and Inhibitor Soaking. Human MTA phosphorylase was overexpressed, purified, and crystallized as described previously (*15*). After 2 weeks of growth, crystals were transferred into an inhibitor soaking solution containing 5 mM formycin A (FMA) or 5′-methylthiotubercidin (MTT) and 15% (w/v) PEG 6000, 25% (v/v) ethylene glycol, and 10 mM $(NH_4)_2SO_4$. The crystals were soaked for 8 h with the soaking solution being replaced every 2 h.

Data Collection and Structure Determination. The crystals were flash-frozen directly without use of further cryoprotection in a stream of nitrogen gas (100 K). Single wavelength (1.000 Å) diffraction data were collected at the Advanced Photon Source, Beamline 32-ID (Argonne National Laboratories, Chicago, IL), on a 165 mm MAR CCD detector. Data were reduced with the help of the program DENZO and scaled using SCALEPACK (*18*). The data collection statistics are shown in Table 1.

The structures of the MTAP−FMA complex and the MTAP−MTT complex were determined by difference Fourier methods using the coordinates of the protein atoms from the MTAP−MTA-sulfate complex (PDB code 1CG6) as the initial model. All rounds of refinement were performed in CNS (*19*) using all data with no σ cutoff and a bulk solvent correction. One cycle of rigid body refinement resulted in the clear identification of the inhibitors in the difference Fourier electron density map. Further torsion angle simulated annealing refinement starting at 5000 K (*20*) was alternated with rounds of manual rebuilding using the interactive computer graphics program "O" (*21*). The progress of the refinement was monitored by reductions in R_{cryst} and R_{free}. The coordinates for FMA and MTT were generated by modifying the PDB files of adenosine and MTA downloaded from the HIC-UP server (*22*), respectively. The topology and parameter files for FMA and MTT were generated using the XPLO2D server (*23*). Water molecules were included into the model during the later rounds of refinement based on the presence of a 3σ peak in the σ_A-weighted $F_o - F_c$ difference electron density map and at least one hydrogen bond to a protein, inhibitor, or solvent atom. The final refinement statistics are shown in Table 1.

Structural Superimpositions. The MTA/AdoHcy nucleosidase (PDB code 1NC1) and MTA phosphorylase structures were aligned by nonlinear least-squares fit of selected main chain (N−C^α−C) atoms in the active sites of the proteins using the program PROFIT (v. 6.0), written by G. David Smith for in-house use. The active site residues used for superimposition were 171−174 and 196−197 in the nucleosidase and 194−197 and 219−220 in the phosphorylase.

Protein Data Bank Accession Codes. The coordinates and X-ray amplitudes of MTAP complexed with FMA and MTT have been deposited in the Protein Data Bank (PDB) (*24*) with accession codes 1SD1 and 1SD2, respectively (http://www.rcsb.org). PDB codes for the FMA- and MTT-complexed nucleosidase structures are 1NC3 and 1NC1, respectively.

RESULTS AND DISCUSSION

Structural Determination. MTA phosphorylase was crystallized as described previously (*15*). The MTAP−formycin A (MTAP−FMA) and 5′-methylthiotubercidin (MTAP−MTT) complexes were obtained by soaking the inhibitors into the MTAP crystals. The FMA- and MTT-bound phosphorylase crystals diffracted to 2.0 and 2.1 Å resolution, respectively, and contain one molecule in the asymmetric unit. The MTAP−FMA and MTAP−MTT structures were determined using difference Fourier methods and refined to $R_{cryst} = 18.0\%$, $R_{free} = 19.8\%$ and $R_{cryst} = 18.6\%$, $R_{free} = 20.7\%$, respectively (Table 1). Residues 9−281 were modeled into clear electron density in the MTAP−FMA structure; however, in the MTAP−MTT complex residues 128−133 were disordered and omitted from the final model. Analysis of the structures using PROCHECK (*25*) and CNS (*19*) reveals that none of the non-glycine residues fall into the disallowed regions of the Ramachandran plot. Please note, for ease of comparison, that the numbering of atoms in the purine base of the inhibitors FMA and MTT will be based on the numbering convention of MTA and not the IUPAC standard (Figure 2).

Structural Comparison of MTAP Complexes. A superimposition of the MTAP−FMA, MTAP−MTT, and MTAP−

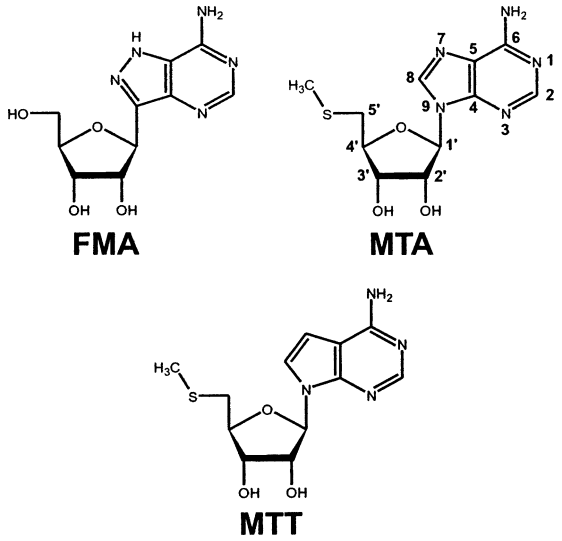

FIGURE 2: Structures of formycin A (FMA), 5′-methylthioadenosine (MTA), and 5′-methylthiotubercidin (MTT). For ease of comparison, the numbering of atoms throughout the text for the purine base of the ligands (MTT and FMA) is based on the numbering convention of MTA and not the IUPAC standard.

MTA complexes shows that the overall main chain and side chain atom positions are nearly identical (mean displacement ~0.3−0.4 Å). Although the MTAP complexes are identical in overall structure, an examination of their active sites reveals key differences. In the MTAP−MTT structure, one key difference is the lengthening of the interactions between the purine ring of MTT and the enzyme. The distance between the Asp220 $O^{\delta 2}$ and the C7 position of MTT is ~3.3 Å, while in the MTAP−FMA and MTAP−MTA complexes, the distances between Asp220 $O^{\delta 2}$ and the equivalent purine N7 are 2.8 and 3.0 Å, respectively (Figures 3a and 4). The repositioning of MTT in the active site results from the inhibitor pulling away from the side chain of Asp220 rather than a reorientation of the side chain and is the result of van der Waals repulsion between the carbon at C7 and the Asp220 oxygen atoms. To compensate for this MTT movement, there is also a reorientation of the sulfate O4 oxygen atom that brings it closer to the C1′ position (3.6 Å) than in the MTA-bound phosphorylase structure (4.2 Å). Another key difference involves the sugar puckering of the MTT nucleoside in MTAP. Nucleosides in MTAP-complexed structures are typical in a higher energy nucleoside C4′-endo pucker conformation with a pucker amplitude of ~35°. FMA and MTT are no exceptions and are also bound with a high-energy C4′-endo sugar pucker conformation. However, the pucker amplitude in MTT is smaller (13°) than those seen in FMA or MTA (~35°). As a consequence of the smaller pucker amplitude in MTT, the 5′-methylthio tail is shifted as compared to the MTA-bound nucleoside. This shift in the 5′-methylthio tail does not alter the torsion angle of the C4′−C5′ bond.

The active site of the MTAP−FMA structure does not contain a sulfate ion (Figures 3a and 4b,d), even though sulfate was present in the soaking solution. Three water molecules, WAT13, WAT28, and WAT32, replace and mimic the O2, O3, and O1 sulfate oxygen atoms, respectively (Figure 4). From the presently available structures, there is no clear structural reason why the sulfate ion cannot bind to the active site in the MTAP−FMA complex. The structural superimposition of the FMA- and MTT-bound MTAP monomers reveals very little main chain deviations (overall mean displacement ~0.35 Å). Furthermore, all residues involved in sulfate binding have similar side chain torsion angles. A possible explanation may reside in the fact that the 5′-methylthio group of MTT, as well as MTA, is nestled in the hydrophobic pocket created by Phe177, Val233, Val236, Leu237, and Leu279 from a neighboring subunit. The presence of the 5′-methylthio group excludes water, whereas the smaller and more polar 5′-hydroxyl group of FMA may favor a water-filled cavity. Disordered and ordered water molecules in this cavity might change the stereoelectronic features of the adjacent phosphate binding site, which would in turn disfavor the binding of phosphate or sulfate. Interestingly, the MTAN−FMA-bound structure also has structural differences in this region. Two different conformations of the putative catalytic base (Glu12) are observed in the two subunits (Figure 3b) (*17*). Glu12 in monomer A is in a catalytically incompetent conformation with the carboxyl oxygens of Glu12 hydrogen bonded to the hydroxyls of Ser218 and Thr74 as well as the amide nitrogens of Gly75 and Ser219. No interaction is seen between the catalytic base (Glu12) and the nucleophilic water (WAT3). The ribose cavity of monomer A contains two extra ordered water molecules than monomer B. In monomer B, Glu12 is thought to be in a catalytically competent conformation as it interacts directly with the nucleophilic water.

Structural Comparison of MTAP and MTAN. The human MTA phosphorylase structures complexed with FMA and MTT are very similar, with an overall main chain mean displacement of ~0.35 Å. The structural comparison of *E. coli* MTA/AdoHcy nucleosidase complexed with FMA (MTAN−FMA) and MTT (MTAN−MTT) also found only small deviations between the two structures (mean displacement = 0.3 Å) (*17*). For ease of comparison we have used the structures of MTT complexed to MTAP and MTAN as the representative models to describe the differences between the two enzymes. The superimposition of MTAP and MTAN revealed an overall mean displacement in the main chain of 3.5 Å (N−C^{α}−C). A displacement plot of the C^{α} atoms in the MTAP−MTT and MTAN−MTT monomeric structures highlights six major regions that deviate by more than 4.0 Å (labeled 1−6 in Figure 5a). Regions 1, 4, 5, and 6 contribute to changes in the active site architecture of MTAP and MTAN. The active sites of MTA/AdoHcy nucleosidase and MTA phosphorylase can be divided into three parts, the adenine/purine, ribose, and 5′-alkylthio binding sites (*15*−*17*). Examination of each of these regions of the active site has revealed a number of differences that account for the enzymes' substrate preferences and which could be exploited to design nucleosidase-specific inhibitors.

Adenine/Purine Binding Site. In the MTT-bound MTAP structure, the purine moiety makes interactions to residues Asp220, Asp222, and Phe177 and a water molecule (WAT1) (Figures 4a and 6a). The Asp220 $O^{\delta 2}$ and Asp222 $O^{\delta 1}$ make hydrogen bonds to the 6-amino group. WAT1 makes hydrogen bond interactions to the N1 purine, while an aromatic herringbone interaction (*26*) is made between Phe177 and the purine base. The Thr219 $O^{\gamma 1}$ and amide nitrogen of Asp222 hydrogen bond to the Asp220 $O^{\delta 1}$ and $O^{\delta 2}$, respectively, and help to correctly orient the Asp220 side chain. In the MTT−MTAN structure, the purine makes

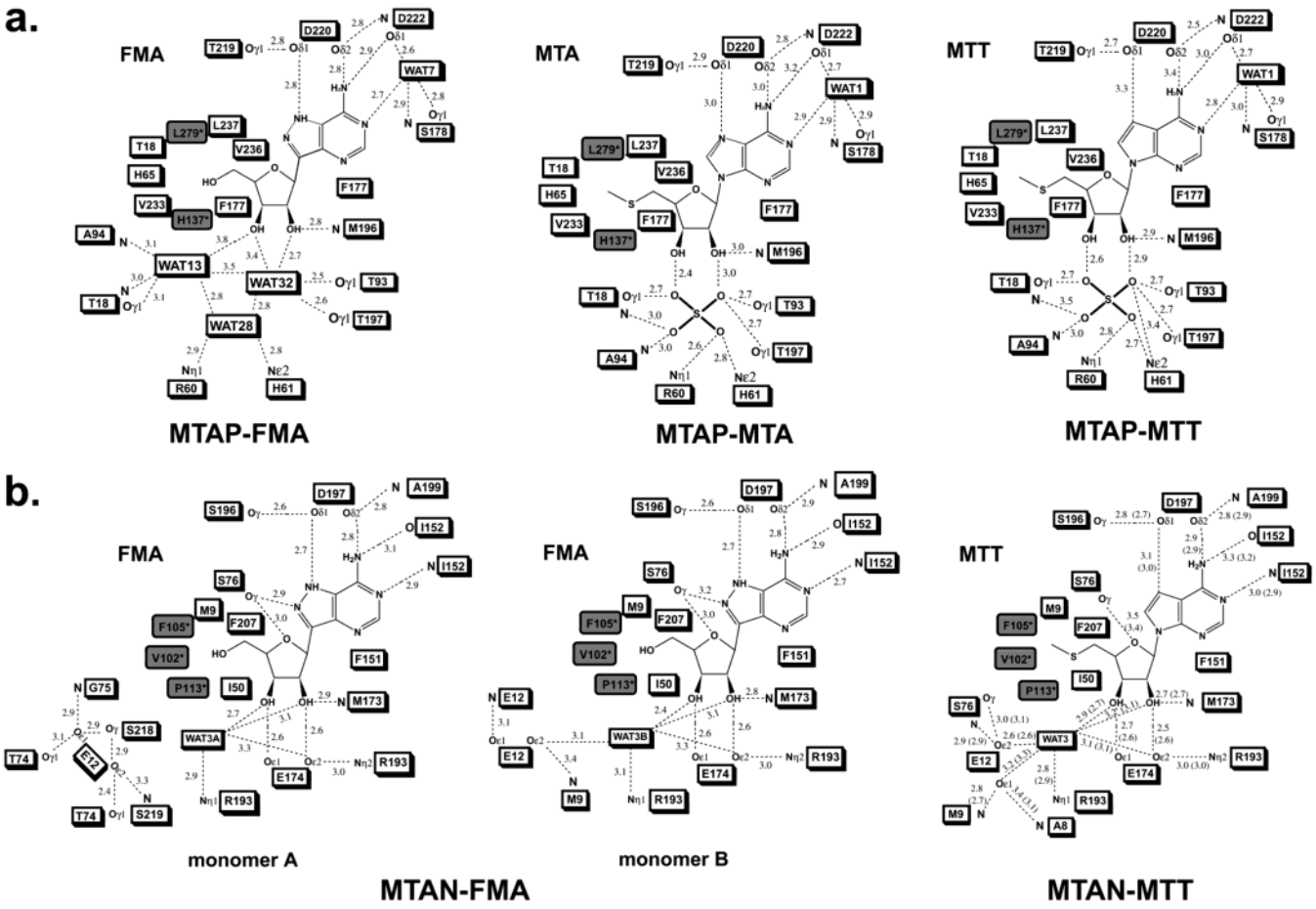

FIGURE 3: Active site schematic comparison of MTA phosphorylase. A schematic of the interactions made in the active sites of the (a) MTAP−FMA, MTAP−MTA (PDB code 1CG6), and MTAP−MTT and (b) MTAN−FMA and MTAN−MTT structures. Residues donated from a neighboring subunit are shaded in a gray box with an asterisk. Dotted lines represent protein−protein, protein−ligand, or protein−solvent hydrogen bonds with distances given in angstroms (Å). Panel b is reprinted with permission from ref *17*. Copyright 2003 Journal of Biological Chemistry.

interactions to residues Asp197, Ile152, and Phe151 (Figures 3b and 6a). The 6-amino group is hydrogen bonded to the Asp197 $O^{\delta 2}$ and the main chain carbonyl oxygen of Ile152. The N1 atom is hydrogen bonded by the amide nitrogen of Ile152. Phe151 makes van der Waals interactions with the purine base. Asp197, like Asp220 in the phosphorylase structure, is held in place by interactions between the carboxyl oxygens and hydroxyl of Ser196 and amide nitrogen of Ala199.

The purine binding sites of MTAP and MTAN are very similar in nature. Both purine binding sites are negatively charged (Figure 6d). This negative potential in MTAP and MTAN will likely repel electronegative substitutions to the purine base. This explains why MTAP has poor affinity for 6-chloropurine (*27*) and why compounds where the N6 amino group has been replaced with a keto group, such as 5′-methylthioinosine, do not serve as substrates or inhibitors for either MTAP or MTAN, respectively (*28*, *29*). The introduction of electronegative substituents will likely be detrimental to binding. One difference that could be exploited to improve affinity is the presence of an extra serine in the purine binding site of MTAN (Figure 3). In the MTT-bound structures of MTAP and MTAN, the purine base is coordinated by three hydrogen bonds. A fourth hydrogen bond would be made between the $O^{\delta 1}$ of either Asp220 (MTAP) or Asp197 (MTAN) and the N7 of a ligand with an intact adenine base. In the MTAN−FMA structure, five hydrogen bonds anchor the purine base. The extra hydrogen bond is formed between the purine N8 and the O^{γ} of Ser76. In the MTAP−MTA structure, the purine makes only four hydrogen bonds as Ser76 is replaced by Ala94 in the phosphorylase, thereby creating a differential in the number of hydrogen bonds. Alternative substitutions at the C8 position, such as an amino group, could also exploit these structural differences between the enzymes, and therefore chemical substitutions at the C8 position need to be explored when trying to design higher affinity, more specific nucleosidase inhibitors.

The biggest difference between the MTAP and MTAN purine binding sites is the size of the cavity. We reported previously that significant conformation changes occur in this region between the MTT and adenine-complexed MTAN structures (*17*). For example, the loop containing residues 148−153, the 150's loop, moves up to 3 Å closer to the purine base upon the binding of the MTT inhibitor. A comparison of the 150's loop and the MTAP equivalent 170's loop, residues 173−179, reveals that the 150's loop in nucleosidase is up to 7 Å closer to the purine moiety than the equivalent C^{α} atoms in MTAP (Figure 5a). As a result, the purine binding cavity is more restricted in the MTAN−FMA and MTAN−MTT structures than in either MTAP or in the adenine-bound MTAN (Figure 6d). The MTAP cavity

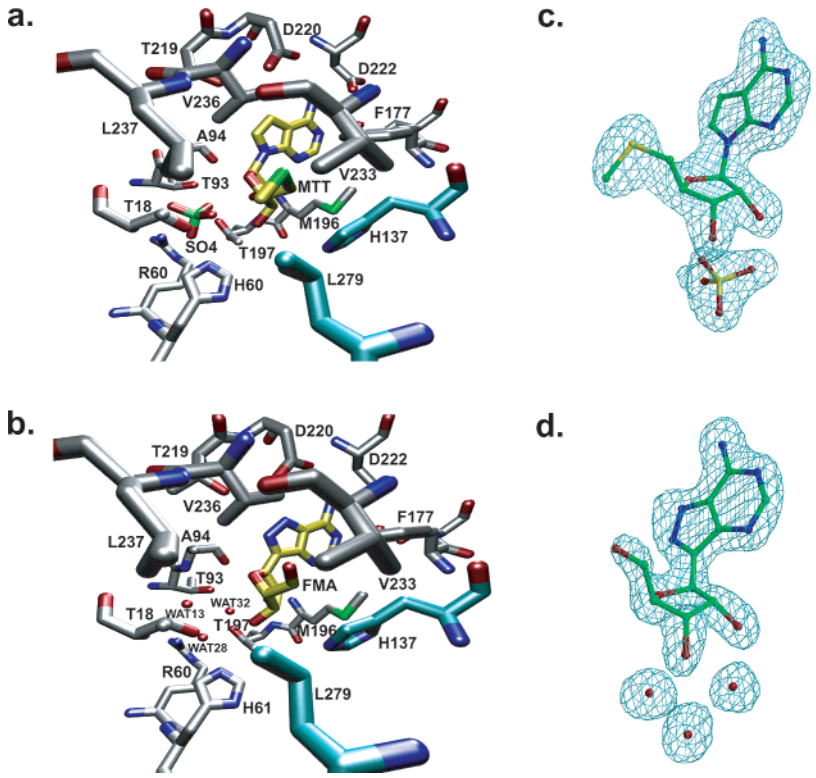

FIGURE 4: Active site comparison of MTAP structures. Stick representation of the human MTAP active site bound with (a) MTT and (b) FMA. Residues donated from a neighboring subunit have cyan-colored carbon bonds. Initial σ_A-weighted $F_o - F_c$ electron density map superimposed with the refined (c) MTT and (d) FMA inhibitors. The electron density maps are contoured at 3σ.

is approximately 20 Å^3 larger than the MTAN cavity, and this would account for MTAP's ability to accommodate exocyclic additions at the C2 position. Nucleobases such as 2-methyladenine ($K_m = 32\ \mu M$) and 2-fluoroadenine ($K_m = 17\ \mu M$) bind to MTAP with an affinity similar to that of the adenine base ($K_m = 20\ \mu M$) (*27*). The 150's loop in MTAN is able to move closer to the purine moiety because Asp222 in MTAP is substituted by a less bulky alanine (Ala199) in the nucleosidase. This alanine substitution in MTAN eliminates steric clashes that would otherwise occur with the 150's loop, specifically with the side chain of Ile152, and allows main chain Ile152 atoms to hydrogen bond with the N1 and N6 positions of the purine. The 170's loop in MTAP does not make any direct hydrogen bonds to the purine base; instead, the amide nitrogen and O$^\gamma$ of Ser178 are involved in an indirect hydrogen bond through a water molecule (WAT1) to the N1 purine position.

Ribose and Sulfate/Phosphate Binding Site. In the MTAP−MTT structure, a sulfate is present in the active site and is thought to mimic its natural ligand, phosphate. The binding of the ribose is primarily mediated by hydrogen bonds from the O2′ and O3′ ribose to the sulfate oxygen atoms (Figures 4a and 6b). In addition, a longer hydrogen bond is made between the amide nitrogen of Met196 and the O2′ ribose (2.9 Å). The sulfate is anchored by hydrogen-bonding interactions from the side chains of Thr18, His61, Arg60, Thr197, and Thr93 and the backbone nitrogen atoms of Thr18 and Ala94. In contrast, the binding of the ribose in the nucleosidase relies on two hydrogen bonds from the O$^{\epsilon 1}$ and O$^{\epsilon 2}$ of Glu174 to the O2′ and O3′ positions, respectively. The nucleophilic water (WAT3) also makes two hydrogen bonds to the ribosyl O2′ and O3′ positions. In the MTAN−MTT structure, WAT3 is further stabilized by hydrogen bonds to the putative catalytic base Glu12, Glu174, and Arg193. Two weaker hydrogen bonds are also made between the amide nitrogen of Met173 and O$^\gamma$ of Ser76 to the ribosyl O2′ and O4′ atoms, respectively.

The ribose binding site is clearly different between MTAP and MTAN (Figure 6b,e). The differences at this binding site explain why the nucleosidase cannot act as a phosphorylase even though the tertiary structure and the active site architecture are so similar. The nucleosidase has a cavity that is approximately the same size as the phosphorylase, but MTAN lacks the ability to coordinate a phosphate anion. In place of the phosphate is the nucleophilic water (WAT3). A phosphate anion is unlikely to bind to the nucleosidase as Thr93 and Thr197 in the phosphorylase have been replaced in the nucleosidase by the bulkier residues Arg193 and Glu174, respectively. In addition, MTAP residues Thr18, Arg60, and His61 are substituted to Met9, Ser48, and Gly49, respectively, in MTAN. The truncation of the Thr18, Arg60, and His61 eliminates the attractive electrostatic and hydrogen-bonding interactions required for phosphate binding. As a consequence of these substitutions, the nucleosidase cavity is predominantly negatively charged near the ribosyl O2′ and O3′ positions (Figure 6e). This negative charge would likely destabilize or repel the anionic phosphate. This reversal in the electrostatic potential could potentially be exploited to create tighter binding and more specific nucleosidase inhibitors. The addition of an electropositive or positively charged group such as a guanidinium moiety at the O2′ position may allow for greater affinity and specificity toward the nucleosidase. A guanidinyl group will likely make a favorable salt bridge to the catalytic base (Glu12) in the nucleosidase and also maintain hydrogen bonds to Glu174. Meanwhile, since the ribose binding site in the phosphorylase is positively

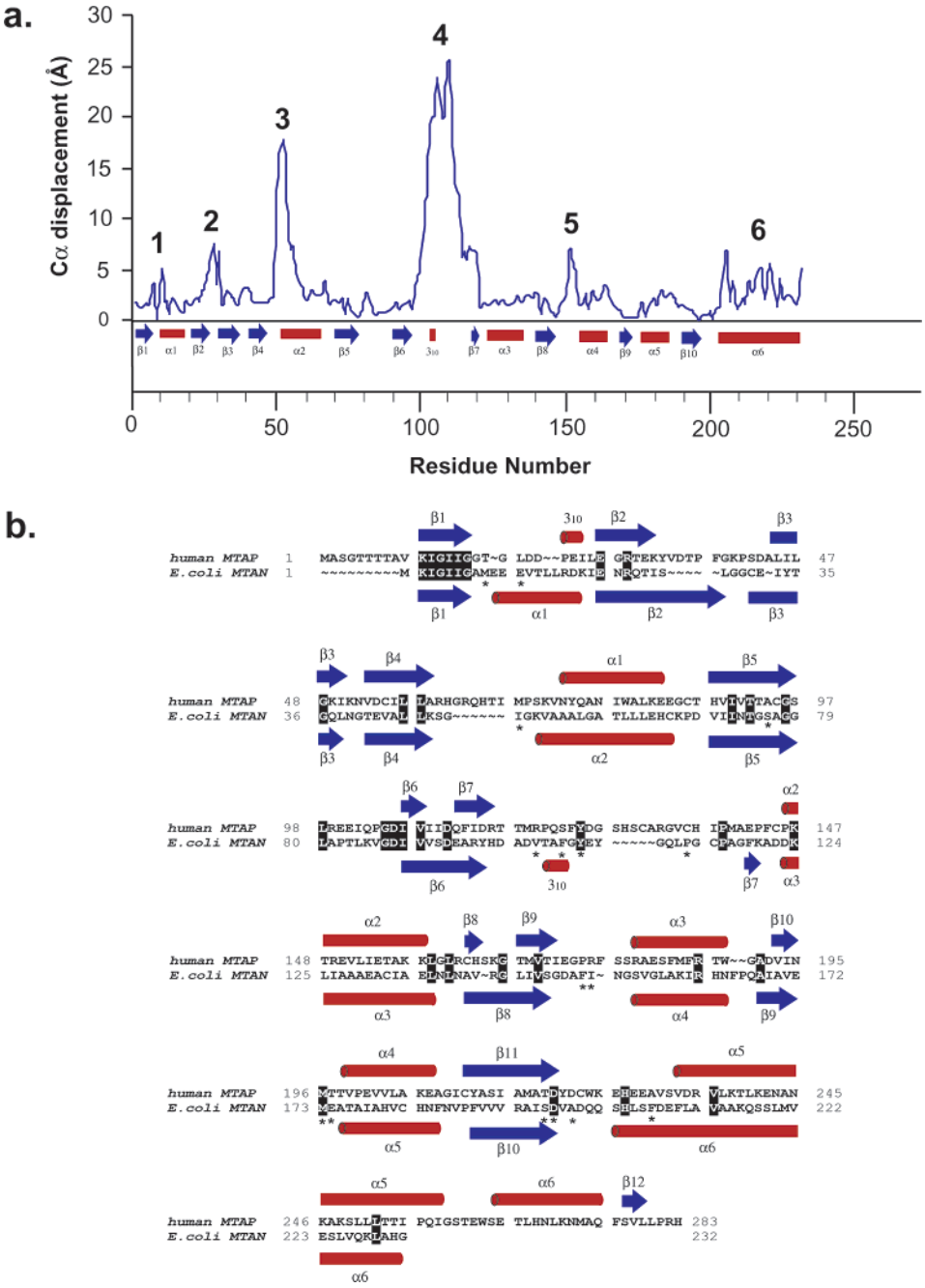

FIGURE 5: Structural comparison of MTAN and MTAP. (a) Mean displacement of Cα positions between monomer A of the MTAN−MTT and MTAP−MTT structures. α-Helices and *β*-sheets are labeled according to the nucleosidase assignment by PROMOTIF (*25*) and are shown as rectangles and arrows, respectively. (b) Structure-based sequence alignment of MTAP−MTT and MTAN−MTT. Secondary structural elements are labeled with α-helices depicted as red cylinders and *β*-strands as blue arrows. The secondary structural elements are assigned using PROMOTIF (*38*). Conserved residues are highlighted in a black box, and MTAN active site residues are labeled with an asterisk.

charged, a 2′-guanidinyl-substituted nucleoside inhibitor will be electrostatically repelled.

5′-Alkylthio Binding Site. In MTAP, the 5′-alkylthio binding site is composed of residues Thr18, His65, His137, Phe177, Val233, Val236, Leu237, and Leu279, with His137 and Leu279 being contributed from a neighboring subunit (Figures 3a and 6c). Residues Thr18, His137, Phe177, Val233, and Val236 form the sides of the cavity, while His65, Leu237, and Leu279 form one end of the hydrophobic pocket. The conformation of the 5′-methylthio tail can be described by two torsion angles describing the C4′−C5′ bond, ϕ_{oo} (S5−C5′−C4′−O4′) and ϕ_{oc} (S5−C5′−C4′−C3′) (*30*, *31*). The MTT in MTAP has a C4′−C5′ bond orientation of $\phi_{oo} = 60°$ and $\phi_{oc} = -179°$. In comparison, the 5′-alkylthio binding site in the nucleosidase is composed of residues Met9, Ile50, Phe151, Met173, and Phe207, and residues Val102, Phe105, Tyr107, and Pro113 from a neighboring subunit (Figure 6c). MTT binds with an exocyclic C4′−C5′ bond orientation of $\phi_{oo} = 167°$ and $\phi_{oc} = -75°$.

The small molecule crystal structure of MTA has an exocyclic C4′−C5′ bond torsion angle of $\phi_{oo} = 169°$ (S5−C5′−C4′−O4′) and $\phi_{oc} = -69.4°$ (S5−C5′−C4′−C3′) corresponding to the *trans*, *gauche* conformation in the two

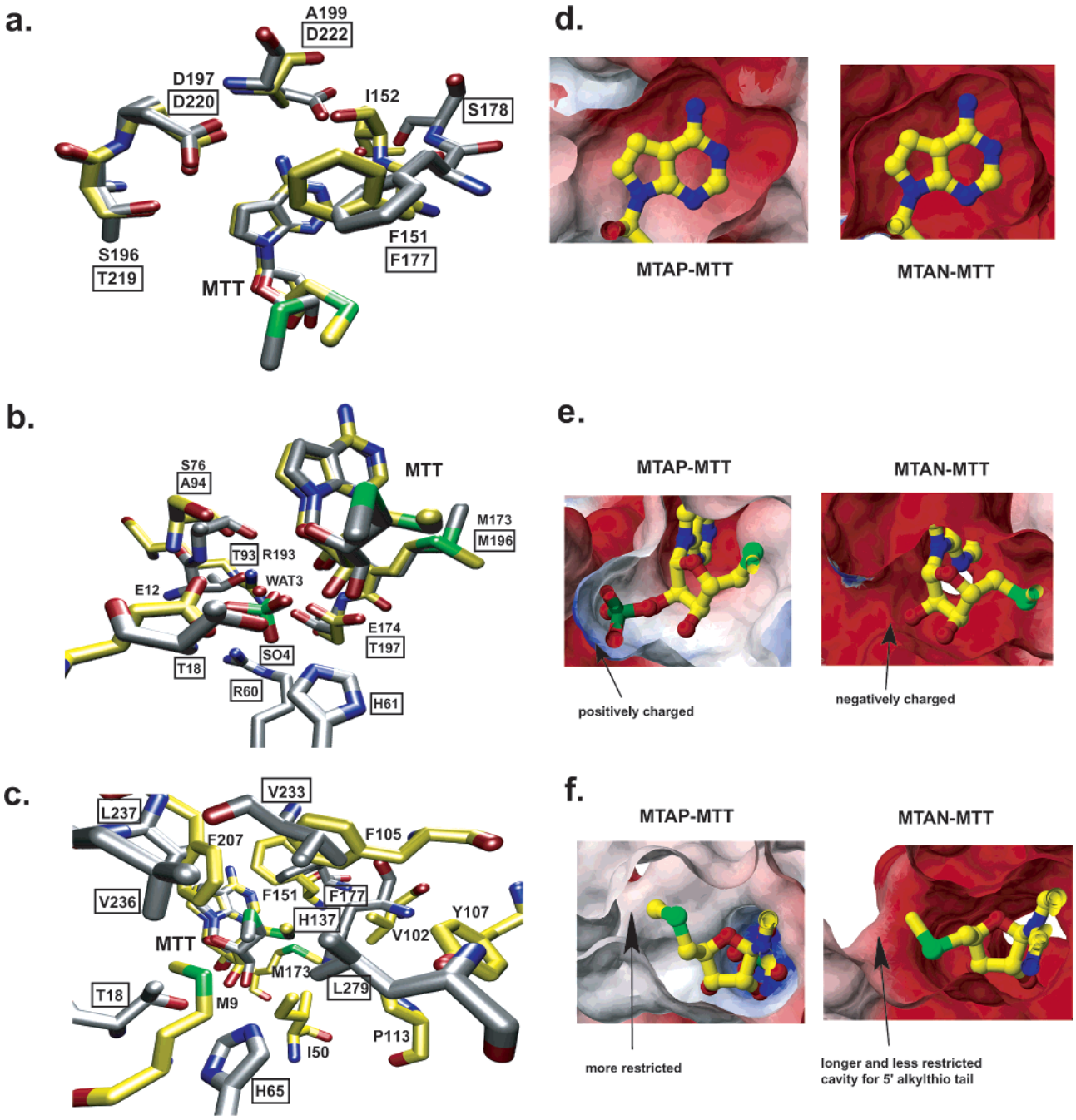

FIGURE 6: Active site comparison. Stick representation of the superimposition of the MTAP and MTAN (a) purine, (b) ribose, and (c) 5′-alkylthio binding site. Amino acid labels shown in square boxes and without boxes correspond to MTAP and MTAN residues, respectively. Residues corresponding to MTAP and MTAN have silver- and yellow-colored bonds, respectively. A comparison of the (d) purine, (e) ribose, and (f) 5′-alkylthio binding cavities in MTAP and MTAN complexed with MTT. Electrostatic charge distributions were calculated by solving the Poisson−Boltzmann equation (*39*) in MOLMOL (*40*). Negative, positive, and neutral electrostatic potentials are colored in red, blue, and white, respectively.

independent molecules in the asymmetric unit (*32*). This is likely to be the low-energy 5′-methylthio conformation as this group does not make any intermolecular crystal contacts under 3.5 Å. Not surprisingly, the average torsion angles observed for MTT in the two monomers of the MTAN−MTT structure are very close to those of the small molecule MTA crystal structure. The 5′-methylthio conformation observed in the phosphorylase is however very different from the solid-state and MTAN-bound conformation of MTA. In all MTAP complexed structures determined to date, the 5′-methylthio torsion angle is approximately $\phi_{oo} = 60°$ and $\phi_{oc} = -179°$. The necessity of the 5′-methylthio torsion angle to change from a low-energy to a higher energy conformation in MTAP is likely a result of steric repulsion by His137. In the phosphorylase, His137 is donated from a neighboring subunit and forms part of the 5′-alkylthio binding site. In the nucleosidase, His137 is replaced to Val102. This substitution eliminates steric hindrances and allows the more energetically favorable $\phi_{oo} = 167°$ and $\phi_{oc} = -75°$ 5′-methylthio conformation to be accommodated. Residues Thr18 and Val236 also make van der Waals contacts to the 5′-alkylthio moiety in MTAP. However, in the nucleosidase Val236 is substituted to a bulkier Phe207 while Thr18 is in the vicinity of Met9 and Glu12. The presence of the bulkier

Met9 and Phe207 therefore prevents the 5′-methylthio conformation seen in MTAP ($\phi_{oo} = 60°$ and $\phi_{oc} = -179°$) from forming.

Interestingly, the small molecule solid-state structure of AdoHcy shows a 5′-alkylthio conformation different from any of the conformations described above. The crystal structure of AdoHcy reveals average exocyclic C4′−C5′ orientations of $\phi_{oo} = -64°$ and $\phi_{oc} = 54°$, corresponding to the *gauche*, *gauche* conformation (*33*). The homocysteinyl moiety is in an extended conformation, but the conformation is highly dependent on hydrogen bonds made between the α-amino and α-carboxyl groups and the neighboring adenine base. The molecular conformations found in the small molecule crystal structure are in good agreement with the preferred conformations observed in solution-state ^{1}H NMR spectroscopy studies (*34*). The binding of AdoHcy in the active site of the nucleosidase will likely be in the *trans*, *gauche* conformation. The AdoHcy conformation should be similar to the 5′-methylthio orientation seen in the MTAN−MTT complex because the *gauche*, *gauche* conformation will likely create steric clashes with the enzyme. The entropic penalty for AdoHcy to bind in a higher energy *trans*, *gauche* conformation may also explain AdoHcy's weaker binding affinity ($K_m = 4.3$ μM) to MTAN than MTA ($K_m = 0.43$ μM) (*28*).

The 5′-alkylthio binding site in MTAP and MTAN is expected to have the greatest structural differences due to the specificities of the enzymes. Both MTAP and MTAN have the ability to cleave MTA, but only MTAN recognizes extended polar and bulky 5′-substituted substrates such as AdoHcy and *p*-nitrophenylthioadenosine (*3*, *28*, *35*). Indeed, there is even a 25-fold improvement in the binding affinity of *p*-nitrophenylthioadenosine relative to MTA for the nucleosidase (*28*). In MTAP, biochemical data reveal that nucleosides with smaller hydrophobic 5′-substituents are preferred (*29*, *36*). Our comparison of human MTA phosphorylase and MTA/AdoHcy nucleosidase reveals structural differences at the 5′-alkylthio binding site that account for these preferences. The phosphorylase has a more restricted 5′-alkylthio binding site due to residues His65, Val233, Leu237, and Leu279. These residues are unique to the phosphorylase and form a cap over the 5′-alkylthio binding pocket. In contrast, the nucleosidase 5′-alkylthio binding site lacks residues that form the restrictive cap and is instead open to the exterior surface (Figure 6f). Substrates with bulky 5′-substituents would be tolerated in the nucleosidase 5′-alkylthio binding site but would make steric clashes with the ends of the 5′-alkylthio pocket in the phosphorylase. The tighter affinity of aromatics in MTAN likely comes from π−π base-stacking or herringbone interactions with the aromatic Phe105, Tyr107, Phe151, and Phe207 residues. In addition, the aromatic para position favors an electron-withdrawing group such as a nitro, chloro, or iodo group (*28*). The *p*-nitro substituent on the aromatic ring is the most favored electron-withdrawing group because it likely mimics the negatively charged carboxyl group of the homocysteinyl tail and may make a favorable hydrogen bond to Tyr107 O^{η}. The use of an aromatic moiety such as *p*-nitrophenyl as a scaffold would be a good starting point for future nucleosidase inhibitor design. A more nucleosidase-specific inhibitor may be designed with the extension of the 5′-aromatic unit by one or two methylene units. This extension would better approximate the extended length of the homocysteinyl tail in AdoHcy and lead to greater steric clashes with residues Thr18, His65, Leu237, and Leu279 that line the end of the 5′-alkylthio binding pocket in MTAP.

Insights into Plant MTA Nucleosidases. The breakdown of the nucleosides MTA and AdoHcy differs in various phyla. As mentioned previously, mammals utilize two separate enzymes, MTA phosphorylase and AdoHcy hydrolase, to catabolize MTA and AdoHcy while bacteria use MTA/AdoHcy nucleosidase. Interestingly, plants catabolize MTA and AdoHcy differently than mammalian and microbial systems. Many plants utilize MTA nucleosidase to cleave MTA to adenine and MTR and AdoHcy hydrolase to breakdown AdoHcy to homocysteine and adenosine. The plant nucleosidase has lost its ability to hydrolyze AdoHcy. Characterization of MTA nucleosidase in *Lactobacillus luteus* seeds reveals an ability to discriminate between analogues with and without an α-amino group at the 5′-alkylthio moiety, as AdoHcy was not cleaved in contrast to *S*-adenosylproprionic acid and *S*-adenosylpropanediol (*37*). Representative plant MTA nucleosidase protein sequences from *Glycine max* (soybeans), *Oryza sativa* (rice), and *Arabidopsis thaliana* (mustard plant) have been aligned with the sequence of the *E. coli* enzyme. This alignment (Figure 7) provides a preliminary look into why plant MTA nucleosidases cannot cleave substrate analogues that lack an α-amino group.

The average sequence identity (∼19%) and similarity (∼45%) between the plant MTAN and *E. coli* MTAN is lower than *E. coli* MTAN aligned with other bacterial nucleosidases. However, plant MTAN still does not have significant sequence similarity with human MTAP. A closer examination of the active site residues reveals that the catalytic residues (Glu12 and Asp197) are invariant, as are the residues involved in coordinating the catalytic water (Arg193 and Glu174). However, residues involved in substrate binding have varying degrees of conservation. In the three plant species, residues Ser76 and Ser196 are conservatively substituted to threonine. Interestingly, human MTAP also utilizes a threonine at position 196 to stabilize the catalytic aspartic acid. A larger change is observed in plant MTAN at position 151 with a substitution to leucine (phenylalanine in the *E. coli* enzyme). The leucine substitution will eliminate the base-stacking interactions with the adenine ring observed in both MTAP and MTAN but may still make van der Waals contacts with the base. The other purine and ribose binding site residues that interact through their side chains are fairly well conserved between both the plant and microbial enzymes.

As expected, the greatest sequence variation occurs with residues in the 5′-alkylthio binding site. Residues Met9, Ile50, Val102, Phe105, Tyr107, Pro113, Phe151, and Phe207 in *E. coli* MTA/AdoHcy nucleosidase form the 5′-alkylthio binding site and make van der Waals interactions to the 5′-alkylthio moiety of the substrate. The hydrophobic nature of residues Met9, Ile50, Val102, Phe151, and Phe207 is maintained in the aligned plant nucleosidase species. However, residues that are donated from a neighboring subunit (Val102, Phe105, Tyr107, and Pro113) are variable. In plant MTA nucleosidases, Val102 and Phe105 are replaced by isoleucine and proline, respectively. The β6−α3 loop, which

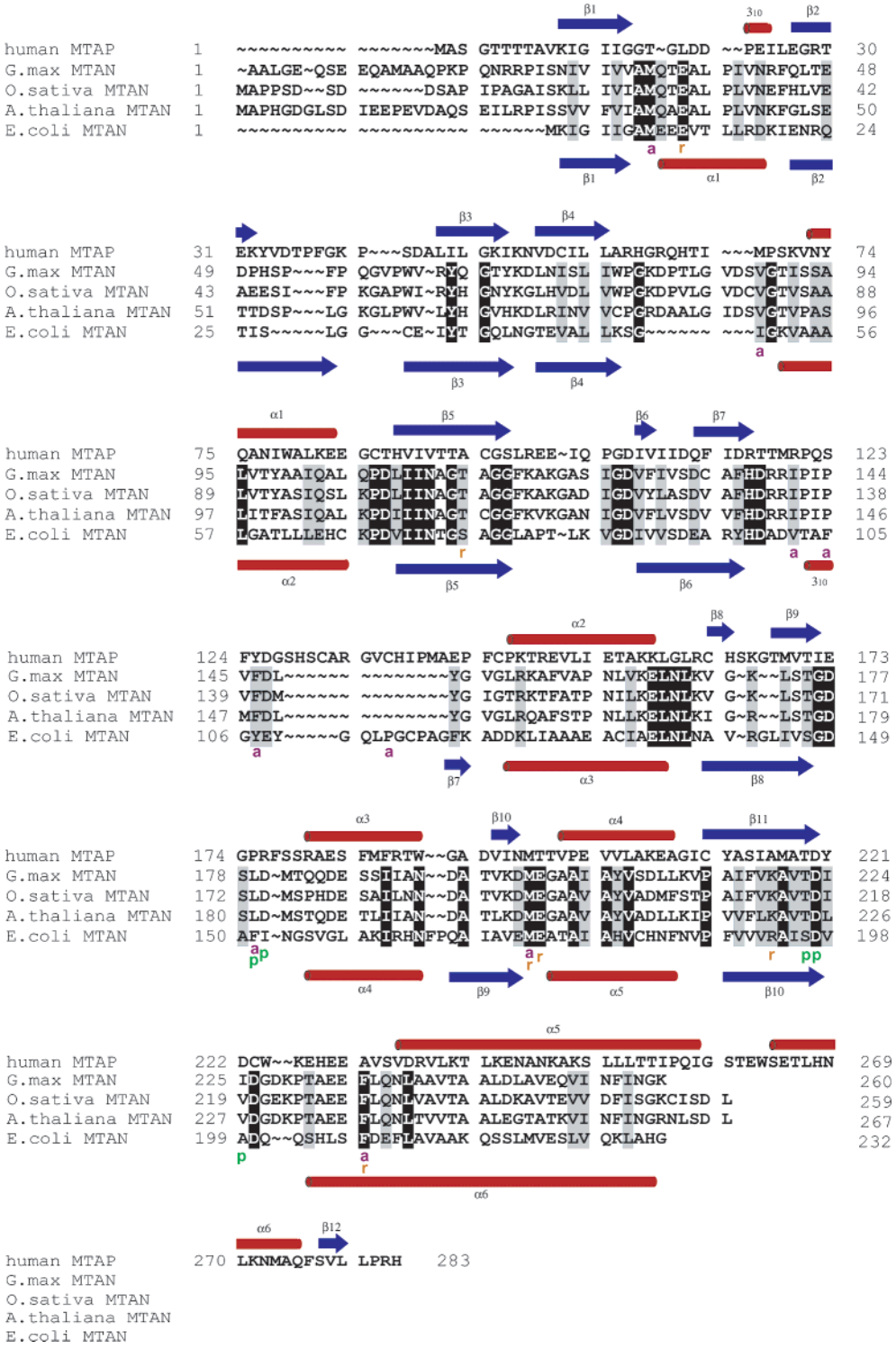

FIGURE 7: Sequence alignment of *E. coli* MTA/AdoHcy nucleosidase and plant MTA nucleosidases. Residues involved in substrate binding in the purine, ribose, and 5′-alkylthio binding sites are labeled p, r, and a, respectively. The primary sequence alignment was performed in the program BioEdit using the ClustalW multiple alignment algorithm (*41*). Boxes highlighted in black show conserved sequences. The human MTAP sequence is structurally aligned to *E. coli* MTAN (see Figure 5b) and is included for comparison purposes only. α-Helices and *β*-sheets were assigned and labeled according to Figure 5b.

contains Pro113, is also truncated by nine residues in the plant species. As a consequence of these changes, the 5′-alkylthio binding site is likely a little larger in plant MTAN than in *E. coli* MTAN and human MTAP and therefore should allow the plant MTAN to bind bulkier 5′-substituted analogues. The ability of plant MTA nucleosidases to discriminate between substrates with a 5′-alkylthio α-amino group may lie in the replacement of the tyrosine at position 107 with phenylalanine. Tyr107 is proposed to make a hydrogen bond interaction to either the α-amino or α-carboxyl groups of the homocysteinyl moiety of AdoHcy in *E. coli* MTA/AdoHcy nucleosidase (*17*). The lack of the O^{η} atom at position 107 could destabilize the binding of AdoHcy by leaving an unsatisfied hydrogen bond to the α-amino group. We are currently in the process of determining the kinetics of site-directed mutants and the crystal structure of

a MTA nucleosidase from the plant phyla to verify our hypothesis.

ACKNOWLEDGMENT

The authors thank Dr. G. David Smith for the program PROFIT (v. 6.0) and Todd C. Appleby for help with protein purification. We also thank the COM-CAT beamline 32-ID of the Advanced Photon Source, Argonne National Laboratories, for providing data collection access.

REFERENCES

1. Sufrin, J. R., Meshnick, S. R., Spiess, A. J., Garofalo-Hannan, J., Pan, X. Q., and Bacchi, C. J. (1995) *Antimicrob. Agents Chemother. 39*, 2511−2515.
2. Riscoe, M. K., Ferro, A. J., and Fitchen, J. H. (1989) *Parasitol. Today 5*, 330−333.
3. Duerre, J. A. (1962) *J. Biol. Chem. 237*, 3737−3741.
4. de la Haba, G., and Cantoni, G. (1959) *J. Biol. Chem. 234*, 603−608.
5. Pajula, R. L., and Raina, A. (1979) *FEBS Lett. 99*, 343−345.
6. Raina, A., Tuomi, K., and Pajula, R. L. (1982) *Biochem. J. 204*, 697−703.
7. Borchardt, R. T., Creveling, C. R., and Ueland, P. M. (1986) *Biological methylation and drug design-Experimental and clinical roles of S-adenosylmethionine*, Humana Press, Clifton, NJ.
8. Passador, L., Cook, J. M., Gambello, M. J., Rust, L., and Iglewski, B. H. (1993) *Science 260*, 1127−1130.
9. Jones, S., Yu, B., Bainton, N. J., Birdsall, M., Bycroft, B. W., Chhabra, S. R., Cox, A. J., Golby, P., Reeves, P. J., Stephens, S., et al. (1993) *EMBO J. 12*, 2477−2482.
10. Fuqua, C., Winans, S. C., and Greenberg, E. P. (1996) *Annu. Rev. Microbiol. 50*, 727−751.
11. Singh, P. K., Schaefer, A. L., Parsek, M. R., Moninger, T. O., Welsh, M. J., and Greenberg, E. P. (2000) *Nature 407*, 762−764.
12. Schauder, S., Shokat, K., Surette, M. G., and Bassler, B. L. (2001) *Mol. Microbiol. 41*, 463−476.
13. Chen, X., Schauder, S., Potier, N., Van Dorsselaer, A., Pelczer, I., Bassler, B. L., and Hughson, F. M. (2002) *Nature 415*, 545−549.
14. Chen, S.-J., Margosiak, S., Feher, V., Pinko, C., Zaidi, S., and Appelt, K. (2002) in *42nd Interscience Conference on Antimicrobial Agents and Chemotherapy*, p F742, American Society for Microbiology, San Diego.
15. Appleby, T. C., Erion, M. D., and Ealick, S. E. (1999) *Structure 7*, 629−641.
16. Lee, J. E., Cornell, K. A., Riscoe, M. K., and Howell, P. L. (2001) *Structure 9*, 941−953.
17. Lee, J. E., Cornell, K. A., Riscoe, M. K., and Howell, P. L. (2003) *J. Biol. Chem. 278*, 8761−8770.
18. Otwinowski, Z., and W, M. (1997) *Methods Enzymol. 276*, 307−326.
19. Brunger, A. T., and Warren, G. L. (1998) *Acta Crystallogr. D54*, 905−921.
20. Brunger, A. T., Krukowski, A., and Erickson, J. W. (1990) *Acta Crystallogr. A46*, 585−593.
21. Jones, T. A., Zou, J. Y., Cowan, S. W., and Kjeldgaard (1991) *Acta Crystallogr. A47* (Part 2), 110−119.
22. Kleywegt, G. J., and Jones, T. A. (1998) *Acta Crystallogr. D54*, 1119−1131.
23. Kleywegt, G. J. (1995) *CCP4/ESF-EACBM Newsletter on Protein Crystallography 31* (June 1995), 45−50.
24. Berman, H. M., Westbrook, J., Feng, Z., Gilliland, G., Bhat, T. N., Weissig, H., Shindyalov, I. N., and Bourne, P. E. (2000) *Nucleic Acids Res. 28*, 235−242.
25. Laskowski, R. A., MacArthur, M. W., Moss, D. S., and Thornton, J. M. (1993) *J. Appl. Crystallogr. 26*, 283−291.
26. Burley, S. K., and Petsko, G. A. (1985) *Science 229*, 23−28.
27. Toorchen, D., and Miller, R. L. (1991) *Biochem. Pharmacol. 41*, 2023−2030.
28. Cornell, K. A., Swarts, W. E., Barry, R. D., and Riscoe, M. K. (1996) *Biochem. Biophys. Res. Commun. 228*, 724−732.
29. White, M. W., Vandenbark, A. A., Barney, C. L., and Ferro, A. J. (1982) *Biochem. Pharmacol. 31*, 503−507.
30. Saenger, W. (1984) *Principles of Nucleic Acid Structure*, Springer-Verlag, New York.
31. Shefter, E., and Trueblood, K. N. (1965) *Acta Crystallogr. A18*, 1067−1077.
32. Borkakoti, N., and Palmer, R. A. (1978) *Acta Crystallogr. B34*, 867−874.
33. Ishida, T., Morimoto, H., and Inoue, M. (1981) *J. Chem. Soc., Chem. Commun. 14*, 671−673.
34. Follmann, H., and Gremels, G. (1974) *Eur. J. Biochem. 47*, 187−197.
35. Della Ragione, F., Porcelli, M., Carteni-Farina, M., Zappia, V., and Pegg, A. E. (1985) *Biochem. J. 232*, 335−341.
36. Bacchi, C. J., Sufrin, J. R., Nathan, H. C., Spiess, A. J., Hannan, T., Garofalo, J., Alecia, K., Katz, L., and Yarlett, N. (1991) *Antimicrob. Agents Chemother. 35*, 1315−1320.
37. Guranowski, A. B., Chiang, P. K., and Cantoni, G. L. (1981) *Eur. J. Biochem. 114*, 293−299.
38. Hutchinson, E. G., and Thornton, J. M. (1996) *Protein Sci. 5*, 212−220.
39. Nicholls, A., and Honig, B. (1990) *J. Comput. Chem. 12*, 435−445.
40. Koradi, R., Billeter, M., and Wuthrich, K. (1996) *J. Mol. Graphics 14*, 29−32, 51−55.
41. Thompson, J. D., Higgins, D. G., and Gibson, T. J. (1994) *Nucleic Acids Res. 22*, 4673−4680.

BI035492H